

Topological Transition to a Critical Phase in a Two-dimensional 3-Vector Model with non-Abelian Fundamental Group: A Simulational Study

B. Kamala Latha¹ and V.S.S. Sastry²

¹*School of Physics, University of Hyderabad, Hyderabad 500046, India and*

²*Centre for Modelling, Simulation and Design, University of Hyderabad, Hyderabad 500046, India*

(Dated: May 20, 2020)

Two-dimensional 3-vector ($d=2, n=3$) lattice model with inversion site symmetry and fundamental group of its order-parameter space $\Pi_1(\mathcal{R}) = Z_2$, did not exhibit the expected topological transition despite stable defects associated with its uniaxial orientational order. This model is investigated specifically requiring the medium to host distinct classes of defects associated with the three ordering directions, facilitating their simultaneous interactions. The necessary non-Abelian isotropy subgroup of \mathcal{R} is realized by assigning D_2 site symmetry, resulting in $\Pi_1(\mathcal{R}) = \mathbb{Q}$ (the group of quaternions). With liquid crystals serving as prototype model, a general biquadratic Hamiltonian is chosen to incorporate equally attractive interactions among the three local directors resulting in an orientational order with the desired topology. A Monte Carlo investigation based on the density of states shows that this model exhibits a transition, simultaneously mediated by the three distinct defects with topological charge $1/2$ (disclinations), to a low-temperature critical state characterized by a line of critical points with quasi-long range order of its directors, their power-law exponents vanishing as temperature tends to zero. It is argued that with $n=3$, simultaneous participation of all spin degrees through their homotopically inequivalent defects is necessary to mediate a transition in the two-dimensional system to a topologically ordered state.

PACS numbers: 64.70.M-, 64.70.mf

In 2-dimensional lattice systems with 3-dimensional spin degrees of freedom, ($d=2, n=3$) models, symmetry of the Hamiltonian impacts its order parameter space (\mathcal{R}) topology [1], requiring non-trivial first fundamental group $\Pi_1(\mathcal{R})$ to sustain stable topological point defects. With a choice of minimal local site symmetry Z_2 , \mathcal{R} is isomorphic to RP^2 (3-d real projective space, $\Pi_1(\mathcal{R}) = Z_2$) resulting in an apolar uniaxial order (in the direction of symmetry), forming stable point-defects (disclinations). Monte Carlo (MC) studies on such models could not establish the presence of a Berenzskii-Kosterlitz-Thouless-type (BKT) transition mediated by topological defects [2, 3], with examples from liquid crystals (LC)[4–8] and magnetic systems [9]. In a related MC study based on density of states [10], it was observed that the initial progression of the system towards such a transition was interrupted by a crossover arising from competing length scales in the system. We investigate this system by requiring that its order-parameter topology allows for a (discrete) non-Abelian fundamental group resulting in distinct classes of topological defects associated with all the spin degrees.

We assign D_2 symmetry to the lattice sites (instead of $D_{\infty h}$ of the earlier model), and augment the Lebwohl-Lasher (LL) Hamiltonian [11] (representing an attractive biquadratic interaction among, say, molecular z-axes), with similar attractive biquadratic interactions among the molecular x-axes and y-axes. The corresponding \mathcal{R} is represented by the space of cosets $SU(2)/\mathbb{Q}$, where $SU(2)$ is the special unitary group of 2×2 matrices and \mathbb{Q} is the discrete non-Abelian group of quaternions. In this case, $\Pi_1(\mathcal{R}) = \mathbb{Q}$, represented by $(\pm 1, \pm i\sigma_x, \pm i\sigma_y, \pm i\sigma_z)$;

(σ_i) is the set of Pauli matrices. The higher order groups are not relevant to 2d models. The medium hosts four types of stable topological defect structures: three distinct types of disclinations (charge $1/2$), corresponding to the order directors associated with the three molecular axes and homotopically equivalent topological defects of unit charge formed by each of the axes [1].

We define two orthogonal (uniaxial and biaxial) molecular tensors, \mathbf{q} and \mathbf{b} respectively, as $\mathbf{q} := \mathbf{m} \otimes \mathbf{m} - \frac{I}{3}$ and $\mathbf{b} := \mathbf{e} \otimes \mathbf{e} - \mathbf{e}_\perp \otimes \mathbf{e}_\perp$ where $(\mathbf{e}, \mathbf{e}_\perp, \mathbf{m})$ is an orthonormal set of vectors representing the molecular axes (in conventional notation [12]). The general biquadratic attractive interaction between two lattice sites is given by $H = -U[\xi \mathbf{q} \cdot \mathbf{q}' + \gamma(\mathbf{q} \cdot \mathbf{b}' + \mathbf{q}' \cdot \mathbf{b}) + \lambda \mathbf{b} \cdot \mathbf{b}']$. This Hamiltonian, setting $\xi = 1$, was extensively examined in three dimensional systems in the parameter space of (γ, λ) , to elucidate its phase diagram [12–15]. We set $\gamma = 0$ hereafter to avoid cross-coupling interactions, without loss of generality. H can be expressed in terms of inner products of the molecular axes $(\mathbf{e}, \mathbf{e}_\perp, \mathbf{m})$, indexing them as (1,2,3) for convenience. The pair-wise interaction between two lattice sites (α, β) then simplifies to $H_{\alpha\beta} = -U\{\xi G_{33} + \lambda [2(G_{11} + G_{22}) - G_{33}]\}$. Here $G_{ij} = P_2(f_{ij})$, $P_2(\cdot)$ denoting the second Legendre polynomial and $f_{ij} = (\mathbf{u}_i \cdot \mathbf{v}_j)$ where $(\mathbf{u}_i, i = 1, 2, 3)$ and $(\mathbf{v}_j, j = 1, 2, 3)$ are the two triads of molecular axes on the sites (α, β) respectively [16]. Reduced temperature (T) is defined in units of U . With the choice of model parameters $\xi=1$ and $\lambda = \frac{1}{3}$ the model exhibits cyclic permutation symmetry with respect to the indices of the local directors, imparting equally attractive interaction among the three axes. This choice leads to the strongest first-order

transition directly from isotropic (disordered) phase to a state with three ordering directions (biaxial phase) [13].

The MC simulations are carried out adopting the Wang-Landau algorithm, to calculate the density of states of the system, and hence extract equilibrium averages of different physical properties of interest (as described in [14, 15, 17, 18]) at 10^3 temperatures over the range [0.1 to 1.5]. We consider interactions of the nearest neighbour sites on 2d square lattices with different sizes $L \times L$, ($L = 60, 80, 100, 120, 150$) and apply periodic boundary conditions. The computed properties include the averages of energy per site (E), the specific heat C_v , the uniaxial (R_{00}^2) and biaxial (R_{22}^2) orientational order parameters, as well as their susceptibilities χ_{00}^2 and χ_{22}^2 [14]. In addition, we also computed the topological parameters of the dominant charge 1/2 defects of the three order directors. The fourth permissible charge 1 defect is difficult to be detected due to energetic reasons [7, 19].

The topological order parameter μ_z , of the z-axis director forming the charge 1/2 defect, is calculated by assigning a unit vector $\mathbf{s}(\mathbf{r})$ at each site \mathbf{r} on the square lattice representing the local z-director orientation. For each bond $(\mathbf{r}, \mathbf{r}')$ the shortest geodesic connecting the vectors $\mathbf{s}(\mathbf{r})$ and $\mathbf{s}(\mathbf{r}')$ on the unit $(n-1)$ -sphere ($n = 3$) is chosen, thus obtaining a map for a closed loop \mathcal{L} on the lattice to a loop on the manifold RP^2 of this director. The homotopy class of this map is given by $\mathcal{W}(\mathcal{L}) = \prod_{(\mathbf{r}, \mathbf{r}') \in \mathcal{L}} \text{sgn}(\mathbf{s}(\mathbf{r}), \mathbf{s}(\mathbf{r}'))$, the product being sequentially ordered over \mathcal{L} . Topological order μ_z is computed as the ensemble average of $\mathcal{W}(\mathcal{L})$ with periodic boundary conditions in place, and a related parameter is calculated as $\delta_z = (1 - \mu_z)/2$ [4]. We computed the density of unbounded charge 1/2 defects d_z of the director connected with the z-axis, by dividing the lattice into a composition of elementary triangular plaquettes. The above product applied to each plaquette yields a defect finding algorithm: if the ordered product is -1, the plaquette encloses a charge 1/2 defect. The average defect density d_z is calculated from the total count of such isolated defects over the lattice and averaged over the ensemble [7]. The topological parameters of the other two directors ($\delta_x, \delta_y; d_x, d_y$) are similarly computed. Pair correlation functions of the spatial variation of reorientational fluctuations, $G(r_{ij}) = \langle P_2(\cos \theta_{ij}) \rangle$, are computed for the three directors (at $L = 150$) at about 80 temperatures. Statistical errors, estimated based on the Jack-knife algorithm [20], in $E, R_{00}^2, R_{22}^2, \delta_{(x,y,z)}$, and $d_{(x,y,z)}$ are typically of the order of 1 in 10^4 , while higher moments ($C_v, \chi_{00}^2, \chi_{22}^2$) are relatively less accurate (about 8 in 10^3).

Fig. 1 depicts the temperature variation of C_v (per site) which is independent of the system size, unlike in a normal order-disorder transition. The two insets show the size dependence of C_v and the temperature variation of the energy (per site) which is found size independent (within errors). Fig. 2 shows the size dependence of R_{00}^2

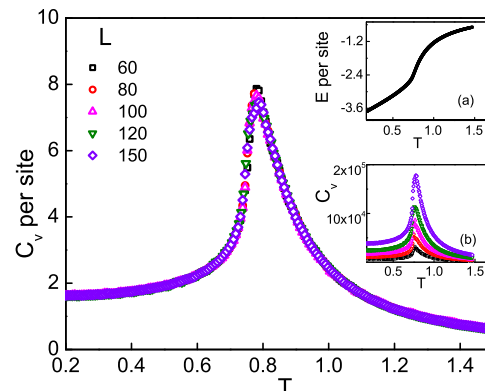


FIG. 1: (color online) Temperature variation of specific heat (per site) at lattice sizes $L = 60, 80, 100, 120, 150$. Insets show the temperature variation of (a) size independent energy per site; (b) size dependence of C_v for different L .

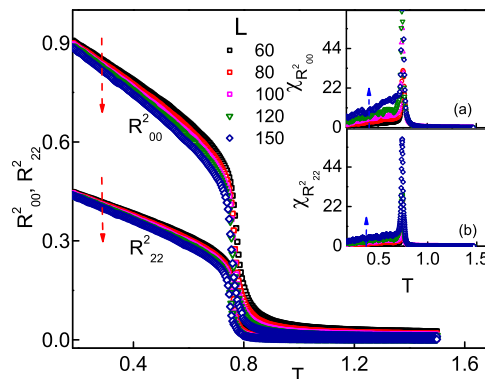


FIG. 2: (color online) Temperature variation of orientational order parameters at lattice sizes $L = 60, 80, 100, 120, 150$. Insets show the temperature variation of (a) uniaxial susceptibility; (b) biaxial susceptibility for different L . (The arrows indicate increase in the size of the system).

and R_{22}^2 , plotted as a function of temperature, and both the order parameters decrease with increase in size. Also the temperatures of their onset are coincident at a given size, shifting to lower values with increase in size. The corresponding susceptibilities (χ_{00}^2, χ_{22}^2), suitably scaled to the system sizes, are depicted in the two insets. The size dependence of peak locations of (χ_{00}^2, χ_{22}^2) are commensurate with the corresponding dependence of onsets of their orders. Their low temperature values below the transition temperatures show a progressive divergence with size (insets of Fig. 2). These features of the orientational orders are typical signatures of a topologically

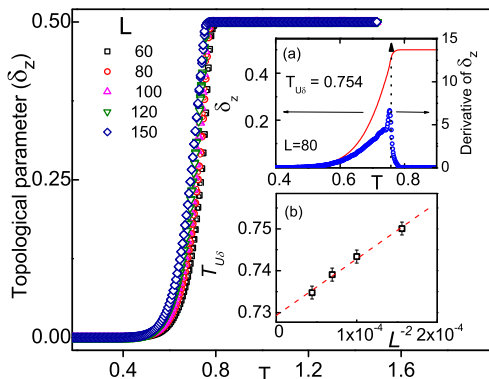


FIG. 3: (color online) Temperature variation of topological parameter δ_z at lattice sizes $L = 60, 80, 100, 120, 150$. Inset (a) shows inflexion point of δ_z at $L = 80$ (dashed vertical line) indicating the unbinding transition temperature $T_{U\delta}$; (b) Finite size scaling plot of $T_{U\delta}(L)$.

ordered medium [6, 21].

The permutation symmetry of the model implies identical variation of the topological parameters ($\delta_x, \delta_y, \delta_z$) and the defect densities (d_x, d_y, d_z) with temperature at a given size, as the present observations confirm. Fig. 3 depicts the size-dependence of the temperature profiles of ($\delta_x, \delta_y, \delta_z$) showing gradual shift to lower temperatures with increase in size, - much like the orientational order profiles and their susceptibility peak positions (see Fig. 2). The inflexion point of the topological order parameter δ with respect to temperature corresponds to the unbinding transition temperature $T_{U\delta}(L)$ and the inset (a) of Fig. 3 depicts its temperature derivative at $L=80$, with a peak at $T_{U\delta}(L)=0.754 (\pm 0.002)$. Inset (b) of Fig. 3 is a finite-size scaling plot of such transition temperatures derived from topological parameter profiles at different sizes, resulting in a reasonable fit and yielding an estimate of the unbinding temperature from this parameter as $T_{U\delta}=0.727 (\pm 0.002)$ in the thermodynamic limit.

The temperature variation profiles of (d_x, d_y, d_z) at different sizes (shown in Fig. 4), essentially collapse to a single curve, except in a very small region near the transition temperature $T_{U\delta} (\simeq 0.727)$. In a topological medium these defects are thermally excited at low temperatures below the unbinding transition (leading to their exponential growth) and proliferate at its onset [22]. Inset(a) of Fig. 4 magnifies temperature variation of the density to depict the slight size-dependence observed near the transition region (shown at $L = 80, 150$). The defect density variation at $L=80$ in this temperature region, along with an exponential fit to data limited to low temperatures ($\leq T_{U\delta}(L = 80)=0.754$), is shown in inset (b), evidencing

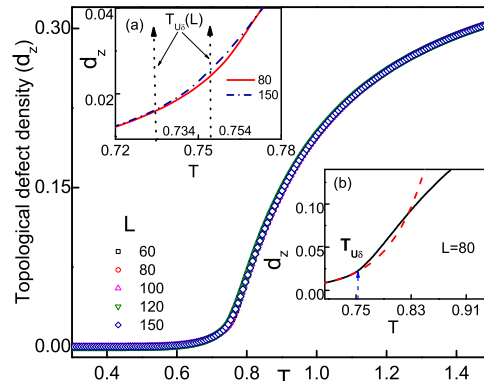


FIG. 4: (color online) Temperature variation of the topological defect density (d_x, d_y, d_z) at lattice sizes $L = 60, 80, 100, 120, 150$. Inset (a) The temperature variations of d_z show their size dependence near critical region (shown at $L = 80, 150$). The dotted vertical lines indicate the values of $T_{U\delta} = 0.734$ and 0.754 at $L = 150$ and 80 respectively; (b) An exponential fit (dashed curve) to the low temperature data superimposed on the temperature variation of d_z (solid line) shows proliferation of defects at $T_{U\delta} \sim 0.75$ at $L=80$.

the onset of proliferation starting near the corresponding unbinding transition temperature.

Spatial variations of $G(r)$ at $L=150$, (depicting only a subset of the data computed at 80 temperatures), are shown in Fig. 5. Each profile represents identical variation of the three directors. For $T \leq 0.73$, the correlation functions obey power law decays very well $G(r, T) \approx r^{-\eta(T)}$, yielding a temperature dependent exponent $\eta(T)$ (within 1% error). $\eta(T)$ is found to vanish as $T \rightarrow 0$, fitting very satisfactorily to the expression $\eta(T) = B(T_{U\eta} - T)^\kappa + \eta_{T_U}$, yielding $T_{U\eta}(L = 150) = 0.729 \pm 0.001$, $\kappa = 0.485 \pm 0.005$, $\eta_{T_U} = 0.342 \pm 0.003$, and $B = 0.399 \pm 0.002$. Here $T_{U\eta}$ is an estimate of the unbinding transition temperature derived from the correlation function data in the low temperature region, comparing well within errors with the corresponding $T_{U\delta} (=0.734)$ at $L = 150$. η_{T_U} is the asymptotic value of the exponent at the transition, and κ is the exponent quantifying vanishing of $\eta(T)$ as $T \rightarrow 0$. The $G(r)$ profiles for $T \geq 0.75$ fit very well to decays given by, $G(r) = A r^{-\eta_{T_U}} \exp[-r/\xi] + A_0$, assigning system length scales $\xi(T)$ (within 2% error) originating from correlations limited by the unbounded defect density in the disordered state. Here A is a non-universal constant, A_0 is related to long-range orientational order, and η_{T_U} is known from the low temperature data. In the small temperature range $[0.73$ to $0.75]$, functional dependence of $G(r)$ could not be assigned satisfactorily to either of the above decay functions with relatively much higher least-square errors, and this region is indicated by two decays

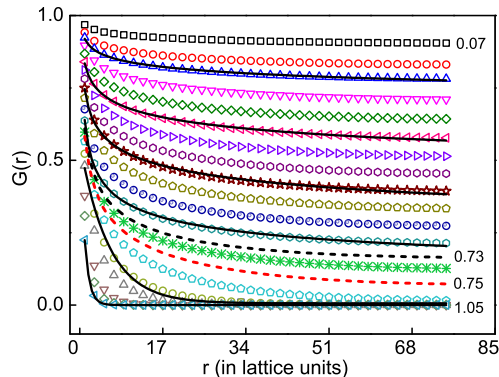


FIG. 5: (color online) Spatial variation of correlation functions $G(r)$ at representative temperatures bracketing the transition ($L = 150$). $G(r)$ fits well to exponential decays above $T = 0.73$, while it exhibits a power law variation below $T = 0.73$. These bounding decays are indicated in the figure as dashed lines. The fit curves both above and below the transition temperature are superimposed on the corresponding data points as solid lines at a few representative temperatures ($T = 0.17, 0.35, 0.53, 0.7, 0.78$ and 1.05).

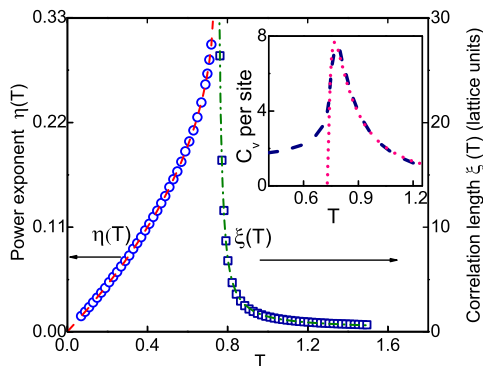


FIG. 6: (color online) Variation of the exponent $\eta(T)$ and $\xi(T)$ with temperature at $L = 150$. The dashed line (left) is the power law fit to $\eta(T)$ and the dash-dotted line (right) is a fit to $\xi(T)$ as indicated in the text. Inset shows the critical contribution to the C_v (short dashes) superposed on the C_v profile (long dashes). The contribution drops to zero at the temperature $T \approx 0.727$ expected of an essential singularity at the transition.

in dashes in Fig. 5.

Fig. 6 plots the variations of $\eta(T)$ and $\xi(T)$ on two abscissae with common temperature ordinate. With the estimated $T_{U\eta}$ value, the divergence of the correlation lengths in the disordered state are fit to $\xi(T) \approx \exp \left[\frac{D}{(T-T_{U\eta})^\nu} \right]$ [3], obtaining $\nu = 0.304 \pm 0.004$. With

these best fit values (at $L = 150$) of $T_{U\eta}$ and ν obtained from the $G(r, T)$ data, critical contribution (arising from the unbinding of defects) to the specific heat profile (together with a background component), given by $C_v \approx \left(\frac{C}{(T-T_{U\eta})} \right)^{2(\nu+1)} \exp \left[-2 \left(\frac{C}{(T-T_{U\eta})} \right)^\nu \right]$ [9, 22] is fit to the variation obtained from MC simulation at $L = 150$ (Fig. 1). The fit parameters are non-universal constants. We note that the critical contribution vanishes as an essential weak singularity at the unbinding temperature. The MC simulated C_v (per site) profile (Fig. 1) is repeated as inset in Fig. 6 (long dashes), plotted along with critical contribution calculated with the above expression, depicted as short dashes. The critical value of C_v is seen to expectedly drop to zero abruptly near the transition temperature. Critical parameters ($T_{U\eta}, \nu$; from Fig. 6) derived from $G(r, T)$ could fairly convincingly generate the observed energy fluctuations above the critical point, based on a topological model of defect-mediated mechanism for the transition. The power law of $G(r, T)$ below $T_{U\eta} (\approx T_{U\delta}) = 0.729$ shows a quasi long range order of the medium, - a critical state.

The present values of η_{T_U} ($= 0.342$) and ν ($= 0.304$) differ from the mean-field values of the 2d XY model, η_c ($= 0.25$) and ν ($= 0.5$). This is to be expected owing to fundamental differences in their \mathcal{R} space topology and $\Pi_1(\mathcal{R})$ groups. Such numerical deviations were observed earlier in systems with $\mathcal{R} \cong RP^2$ (Z_2 site symmetry with $n = 3$) like the case with numerical studies on uniaxial 2d LC model reporting $\eta_c = 0.338$ [21]. Similar argument was advanced to account for this discrepancy in two-dimensional fully frustrated anti-ferromagnetic Heisenberg model on triangular lattice [9].

The results point to the circumstance that, while apolar order is a prerequisite to sustain stable topological defects in $n=3$ model, an enriched order parameter topology engaging all the spin degrees in the formation of distinct defects, backed by suitably chosen Hamiltonian model, is necessary to facilitate their participation in the successful mediation of a topological transition to a critical state. Such choices of topology, requiring a non-Abelian fundamental group, avoid possible onset of other intervening mechanisms, as was encountered in the case of the model with a single class of defects [10].

We acknowledge the computational support from the Centre for Modelling Simulation and Design (CMSD) and the School of Computer and Information Sciences (DST PURSE - II Grant) at the University of Hyderabad. BKL acknowledges financial support from Department of Science and Technology, Government of India vide grant ref No: SR/WOS-A/PM-2/2016 (WSS) to carry out this work.

-
- [1] N. D. Mermin, *Rev. Mod. Phys.* **51**, 591 (1979).
- [2] V. L. Berezenskii, *Sov. Phys. JETP* **32**, 493 (1971); *Sov. Phys. JETP* **34**, 610 (1972).
- [3] J. M. Kosterlitz, and D. J. Thouless, *J. Phys. C* **6**, 1181 (1973).
- [4] H. Kunz and G. Zumbach, *Phys. Rev. B* **46**, 662 (1992).
- [5] B. Berche and R. Paredes, *Condensed Matter Physics*, **8**, 723 (2005).
- [6] E. Mondal and S. K. Roy, *Phys. Lett. A* **312**, 397 (2003).
- [7] S. Dutta and S. K. Roy, *Phys. Rev. E* **70**, 066125 (2004).
- [8] S. Shabnam, S. D. Gupta and S. K. Roy, *Physics Letters A* **380**, 667 (2016).
- [9] H. Kawamura, A. Yamamoto and T. Okubo, *J. Phys. Soc. Japan* **79**, 023701 (2010).
- [10] B. Kamala Latha and V. S. S. Sastry *Phys. Rev. Lett.* **121**, 217801 (2018).
- [11] P. A. Lebowitz and G. Lasher, *Phys. Rev. A* **6**, 426 (1973).
- [12] A. M. Sonnet, E. G. Virga and G. E. Durand, *Phys. Rev. E* **67**, 061701 (2003).
- [13] F. Bisi, E.G. Virga, E.C. Gartland Jr., G.D. Matteis, A.M. Sonnet, and G.E. Durand, *Phys. Rev. E* **73**, 051709 (2006).
- [14] B. Kamala Latha, R. Jose, K. P. N. Murthy and V. S. S. Sastry, *Phys. Rev. E* **92**, 012505 (2015).
- [15] B. Kamala Latha and V. S. S. Sastry, *Liq. Cryst.* **45**, 2197 (2018).
- [16] S. Romano, *Physica A* **337**, 505 (2004).
- [17] F. Wang and D. P. Landau, *Phys. Rev. Lett.* **86**, 2050 (2001); *Phys. Rev. E* **64**, 056101 (2001).
- [18] D. Jayasri, V. S. S. Sastry, and K. P. N. Murthy, *Phys. Rev. E* **72**, 036702 (2005).
- [19] M. Hindmarsh, *Phys. Rev. Lett.* **75**, 2502 (1995).
- [20] B. Kamala Latha, G. Sai Preeti, K. P. N. Murthy and V. S. S. Sastry, *Comp. Mat. Sci.* **118**, 224 (2016).
- [21] A.I. Farinas-Sanchez, R. Botet, B. Berche, and R. Paredes, *Condens. Matter. Phys.* **13**, 13601 (2010).
- [22] R. Kenna, *Condens. Matter. Phys.* **9**, 283 (2006).